



**SYSTEMS TECHNOLOGY, INC**

13766 S. HAWTHORNE BOULEVARD • HAWTHORNE, CALIFORNIA 90250-7083 • PHONE (310) 679-2281  
email: sti@systemstech.com FAX (310) 644-3887

Paper No. 760

**Free Fall Analysis and Simulation Tool  
(FAST)**

April 3, 2011

Thomas T. Myers  
Dongchan Lee, Ph.D.  
Chi-Ying Liang, Ph.D.  
*Systems Technology, Inc.*

Mehila Bozkurttas  
Fady M. Najjar, Ph.D.  
Rajat Mittal, Ph.D

*Cartesian Flow Solutions, Inc., Vienna, VA 22181USA*

Jason Craley  
*Natick Soldier Research, Development and Engineering Center*

AIAA Paper No. 2011-2587

Prepared for:  
21st AIAA Aerodynamic Decelerator Systems  
Technology Conference and Seminar  
Dublin, Ireland  
23 - 26 May 2011



# Free Fall Analysis and Simulation Tool (FAST)

Thomas T. Myers<sup>1</sup>, Dongchan Lee<sup>2</sup> and Chi Liang<sup>3</sup>  
*Systems Technology, Inc., Hawthorne, CA 90250 USA*

Meliha Bozkurttas<sup>4</sup>, Fady M. Najjar<sup>5</sup>, and Rajat Mittal<sup>6</sup>  
*Cartesian Flow Solutions, Inc., Vienna, VA 22181USA*

and

Jason Craley<sup>7</sup>

*Natick Soldier Research, Development and Engineering Center, Natick, MA, 01760USA*

**Military Freefall (MFF), which includes both HALO (High Altitude Low Opening) and HAHO (High Altitude High Opening) operations, is among the most versatile techniques used by Army Airborne Special Forces. The Free Fall Analysis and Simulation Tool (FAST) is being developed to improve understanding of the aerodynamics and dynamics of MFF. FAST is integrated with a Computational Fluid Dynamics (CFD) program, CartFlow3D, which implements the Cartesian grid immersed boundary method to simplify grid generation for complex MFF configurations. Particular emphasis has been devoted to turbulence modeling for the complex and energetic wake. FAST includes a Digital Manikin that simplifies the generation of equipped body shapes in arbitrary poses for input to the CFD program and estimates the mass properties of the parachutist plus equipment. Capability has been implemented to combine the aerodynamic predictions from CFD with the mass properties to analyze free fall stability and control using linearized dynamics. The paper compares CFD results for a parachutist in freefall with no equipment, a chute pack only, and a chute pack plus PDB bag. The longitudinal linearized dynamics of a parachutist in steady freefall are also presented. These show a high frequency complex pitch mode and a lower frequency coupled heave-surge subsidence mode.**

## Nomenclature

$C_x, C_z, C_m$  = aerodynamic coefficients in body axes

$C_L, C_D$  = lift and drag coefficients

$m$  = parachutist mass, equipped

$S$  = parachutist reference area

Re = Reynolds Number

$\bar{u}_i$  = filtered velocity

$\bar{U}_j$  = filtered velocity

---

<sup>1</sup> Sr. Vice President and Technical Director, 13766 S. Hawthorne Blvd, Hawthorne, CA, AIAA Associate Fellow

<sup>2</sup> Senior Research Engineer, 13766 S. Hawthorne Blvd, Hawthorne, CA

<sup>3</sup> Principal Specialist, 13766 S. Hawthorne Blvd, Hawthorne, CA

<sup>4</sup> Research Scientist, Melrose, MA

<sup>5</sup> Scientist, Livermore, CA, AIAA Senior Member

<sup>6</sup> President, Vienna, VA, AIAA Associate Fellow

<sup>7</sup> Aerospace Engineer, PM-CIE, Personnel Airdrop, 15 Kansas St, Bldg 3, R-235, AIAA Member

$U, W$  = surge and heave velocity components, body axes

$x_j$  = position

$\alpha, \beta$  = angles of attack and sideslip

$\nu_e$  = turbulent (eddy) viscosity

$c_v$  = Vreman constant

$B_\beta$  = invariant of matrix  $\beta$

$\beta_{ij}$  = components of the  $\beta$ -matrix in the Vreman Model

$\alpha_{ij}$  = change in velocity with position

$\Delta_m$  = filter width in the m-direction

$\Theta_0$  = equilibrium pitch attitude

$\gamma_0$  = equilibrium flight path angle

$\rho$  = air density

## I. Background and Rationale

Army Airborne Special Forces employ a variety of tactical techniques to execute mission objectives. Among the most versatile is Military Freefall (MFF) which includes both HALO (High Altitude Low Opening) and HAHO (High Altitude High Opening) operations. During HALO operation the parachutist spends 30 sec- 1 min in freefall depending on the desired opening altitude. While this is a brief period, the dynamics of the freefall are critical to mission success. At opening a pilot parachute is first deployed to pull the main canopy from the system harness. Occasionally the pilot parachute fails to enter this airflow and experiences a “hesitation” in which the pilot parachute bridle can easily become entangled and seriously delay or prevent the main canopy from deploying.

Army Special Forces training for Military Freefall HALO and HAHO operations is routinely conducted at the Military Freefall School at Yuma Proving Grounds, AZ. From September 2004 to March 2006 the Military Freefall School noticed a spike in the number of MC-4 main pilot parachute hesitation incidents during student freefall jumps. As a response, the Program Manager-Clothing and Individual Equipment (PM-CIE), Personnel Airdrop Office at the Natick Soldier Research, Development and Engineering Center (Natick Soldier RD&E Center) in Natick, MA initiated an investigation to find the cause of these repeated pilot parachute hesitation incidents.

A peripheral result of this investigation was the conclusion by the Natick Soldier RD&E Center that computer-aided simulation capabilities needed to be developed specifically for freefall analysis. Attempts to use commercially available computational fluid dynamics (CFD) to model MFF were hampered due to the complexity of creating an accurate model of the parachutist in a single pose. An attempt was made to import an image into the software via a 3D body scan but the image redefinition alone proved too time-consuming to continue.

As a response to this capability gap, the Natick Soldier RD&E Center initiated a new topic for the Small Business Innovative Research (SBIR) program entitled “Modeling and Simulation Method to Analyze the Aerodynamic Performance of Paratroopers in Military Freefall Operations”. Following a thorough technical evaluation of all submitted proposals Systems Technology, Inc’s (STI) Freefall Analysis and Simulation Tool (FAST) was selected to receive a six month SBIR Phase I contract award in November 2007 and a Phase II contract in 2008. The following paper summarizes the work accomplished to date by STI and teammate Cartesian Flow Solutions Inc. (CFSI). Further background is presented in Reference 1.

## II. Overview of FAST

The purpose of the Free Fall Analysis and Simulation Tool (FAST, Figure 1) is to provide a means to readily apply the capability of Computational Fluid Dynamics (CFD) to analyze the aerodynamics and dynamics of parachutists in free fall. To do this FAST uses an anthropomorphic model of the human, the "Digital Manikin," which accommodates proper positioning of the head, arms, and legs to greatly simplify the body shape description needed for CFD. An anthropometric database is accessed to compute the mass properties of the parachutist. CFD is then employed to estimate and understand the aerodynamic forces and moments acting on the body in rigid configurations. FAST then applies these aerodynamic forces and moments to the rigid body dynamics of the parachutist to predict his dynamics.

The FAST software does not perform the CFD calculations. Instead it is coupled to a CFD software package, CartFlow3D, specially adapted to the requirements of FAST by CFSI. The FAST Aerodynamics Module provides input parameters to CartFlow3D to initiate CFD runs and receives and processes the output from the CartFlow3D. CartFlow3D has a number of special features which make it ideal for the FAST application. Thus in the following the CartFlow3D software will be discussed first before discussing FAST and its integration with CartFlow3D.

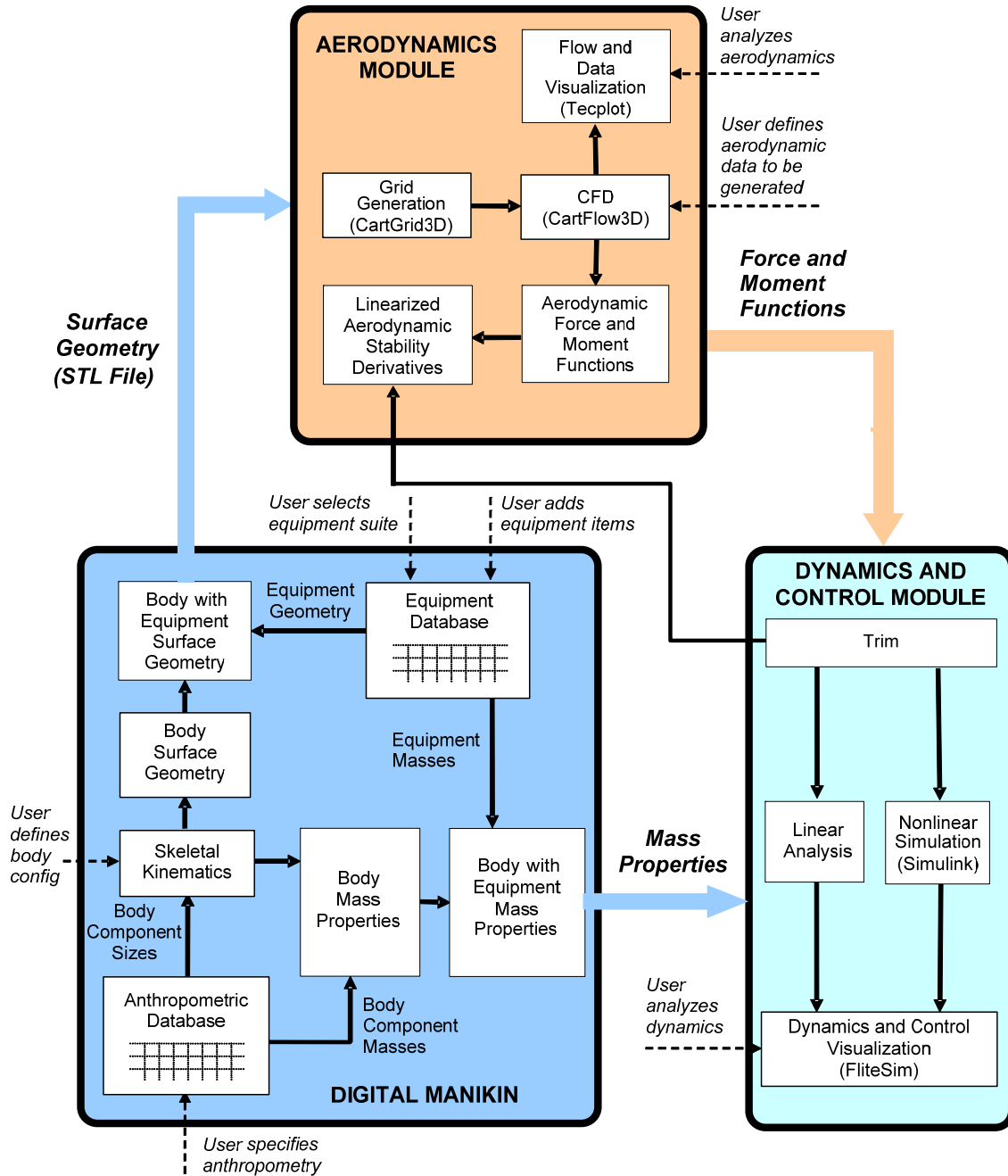


Figure 1 FAST Architecture

### III. CartFlow3D

A key component of the FAST framework is a CFD software, CartFlow3D, which is an incompressible large-eddy simulation (LES) solver based on an immersed boundary method (IBM)<sup>2</sup>. It employs a second-order accurate fractional-step scheme in time and a second-order accurate spatial discretization scheme. The subgrid-scale stress model is formulated using a Vreman's fixed constant model<sup>3</sup> as well as the dynamic version proposed by You and Moin<sup>4</sup>. Validation of CFD results obtained using CartFlow3D with experimental data from water tunnel measurements by Craley & Desabrais<sup>5</sup> which measured drag and wake profiles for three different MFF configurations shows good agreement. These results demonstrated the ability of CartFlow3D to accurately and efficiently model the flow associated with typical MFF configurations.

#### A. Immersed Boundary Method

The current solver is designed from the start for fast, efficient and accurate solution of flows with complex three-dimensional, moving/stationary boundaries. The approach chosen to represent the boundary surface should be flexible enough so as not to limit the type of geometries that can be handled. A number of different approaches are available for representing the surface of the immersed boundary including level-sets<sup>6,7</sup> and unstructured surface grids. In the current solver, we choose to represent the immersed boundary (IB) surface by an unstructured mesh with triangular elements. This approach is very well suited for the wide variety of engineering configurations that we are interested in and is compatible with the immersed boundary methodology used in the current solver.

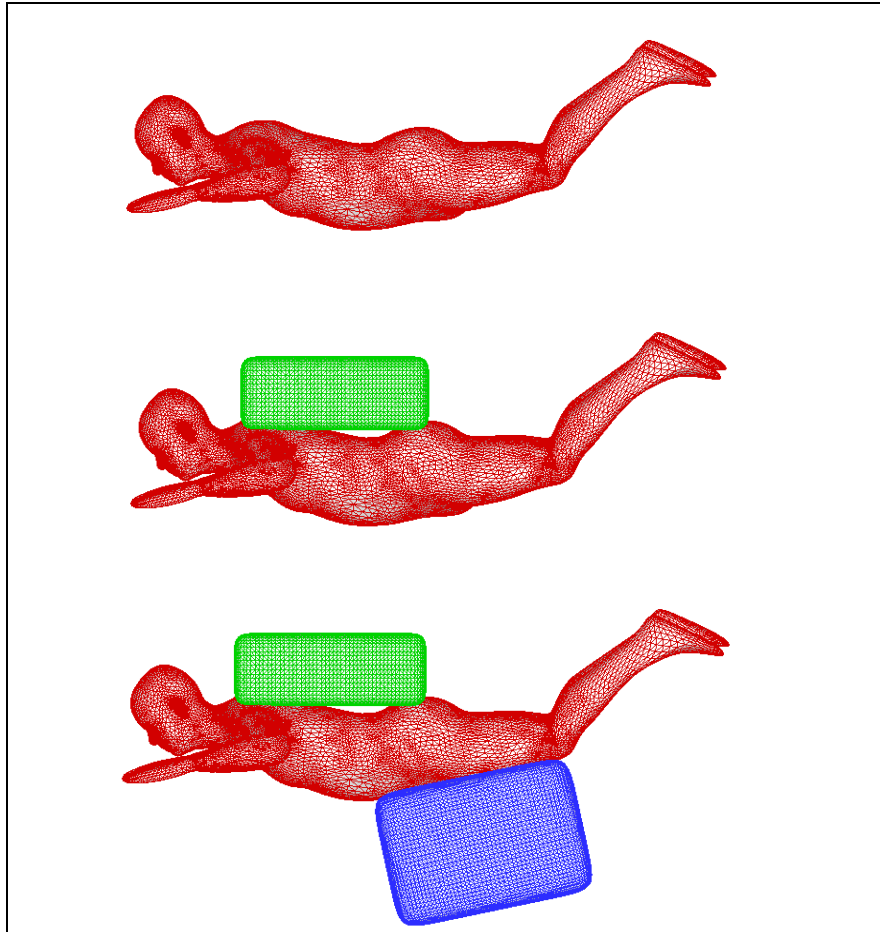


**Figure 2 Surface mesh files for three configurations: Top panel: Case1-No bag; Middle panel: Case 2- Chute pack at rear; Bottom panel: Case 3-Chute Pack at rear and PDB bag in front.**

Different types of interpolation schemes described in literature that are used to implement the boundary conditions corresponding to the immersed body on the Cartesian grid. CartFlow3D uses a simple “stair-step” approximation of the solid boundaries. This significantly reduces the computational expense, and as described in the following section, still produces reasonably accurate results. First, the surface mesh (see Figure 2) is embedded or immersed into the Cartesian grid. Next, a systematic procedure is developed to identify cells whose nodes are inside the solid boundary (termed “solid cells”) and cells that are outside the body (termed “fluid cells”).

## B. LES Turbulence Modeling

The typical speed encountered during MFF is approximately 50 m/s, with the full scale Reynolds number expected to be on the order of about 3 million. The MFF wake is of a turbulent nature, and therefore turbulence models need to be invoked since direct numerical simulation (DNS) is not viable. In our view, conventional Reynolds-Averaged Navier-Stokes (RANS) turbulence models (either steady or unsteady) are quite inappropriate for this effort, since such models have marginal predictive capabilities for separated flows. Particularly, RANS models would impart a high enough eddy-viscosity to the wake so as to damp out even the large-scale vortex structures which are essential to predicting the suction pressure on the lee-side of the body. A better approach is to use a methodology that retains the large-scale vortex structures in the wake, while damping or modeling the finer scale turbulence structures. This is best accomplished through large-eddy simulation (LES) type of approaches.

Several Sub-Grid Scale (SGS) models have been developed that may be used to compute the turbulent eddy viscosity. The simplest SGS model is the Smagorinsky model<sup>8</sup> but the need for ad hoc wall damping<sup>9</sup> to limit excessive dissipation in the near-wall region makes it unsuitable as a candidate for use in complex inhomogeneous flows. To overcome these limitations, the dynamic Smagorinsky model<sup>10</sup> was developed, exhibiting the correct near-wall behavior; however this model requires at least one homogeneous direction for the dynamic procedure to be successful. Meanwhile, the dynamic Lagrangian model eliminates such restrictions on homogeneity by averaging along path-lines making it suitable for use in general flows<sup>11</sup>. However, the selection of model parameters related time scale (needed for the dynamic procedure) in complex three-dimensional flows is not straightforward<sup>11</sup>.

A gradient-based SGS model has recently been introduced by Vreman<sup>3</sup> which is designed to work well in complex three-dimensional flows. Preliminary results show its ability to produce the appropriate near-wall behavior with respect to the eddy viscosity. The Vreman model<sup>3</sup> referred to as VLES, computes the turbulent eddy viscosity in the following manner:

$$\begin{aligned} \nu_e &= C_v \Pi^g, \\ \Pi^g &= \sqrt{\frac{B_\beta^g}{\bar{\alpha}_{ij} \bar{\alpha}_{ij}}}, \\ B_\beta^g &= \beta_{11}^g \beta_{22}^g - \beta_{12}^g \beta_{12}^g + \beta_{11}^g \beta_{33}^g - \beta_{13}^g \beta_{13}^g + \beta_{22}^g \beta_{33}^g - \beta_{23}^g \beta_{23}^g, \\ \beta_{ij}^g &= \sum_{m=1}^3 \bar{\Delta}_m^2 \bar{\alpha}_{mi} \bar{\alpha}_{mj}, \\ \bar{\alpha}_{ij} &= \frac{\partial \bar{u}_j}{\partial x_i} \end{aligned}$$

with  $c_v$  being the Vreman constant,  $c_v \sim 2.5C_s^2$ ,  $C_s = 0.17$ . The superscript  $g$  denotes the grid filter associated with the grid level length scale,  $\Delta$ . A recent enhancement proposed by You & Moin<sup>4</sup> computes the Vreman constant in a dynamic manner; hence it is referred to as DVLES. A validation study<sup>12</sup> has been completed for several canonical flows including turbulent channel flow and flow past a circular cylinder.

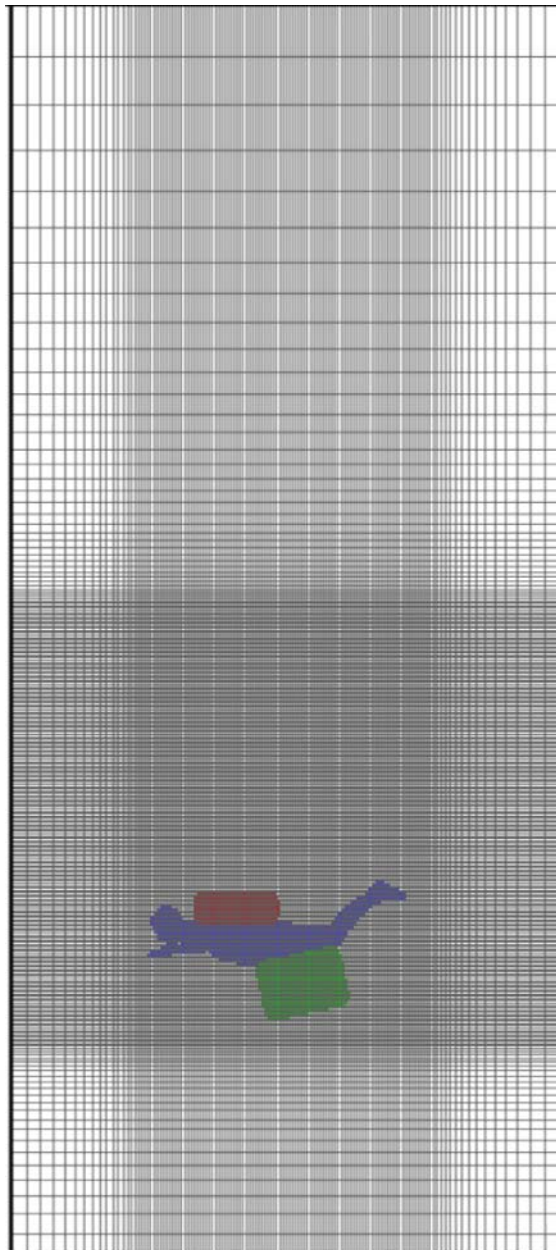
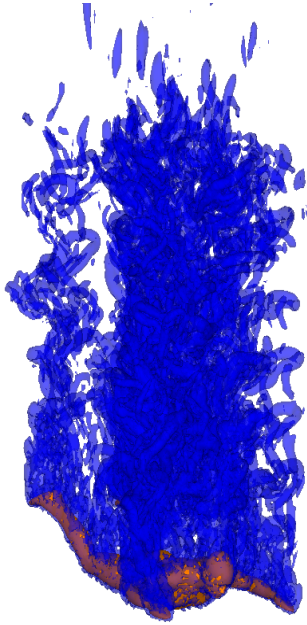
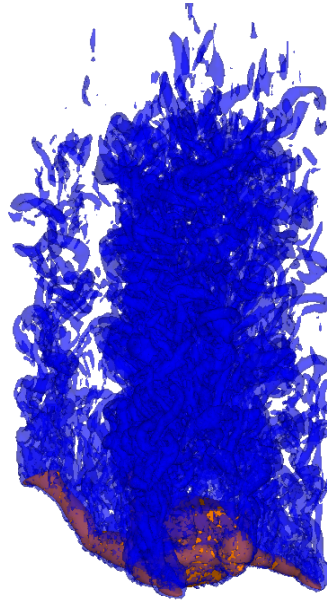


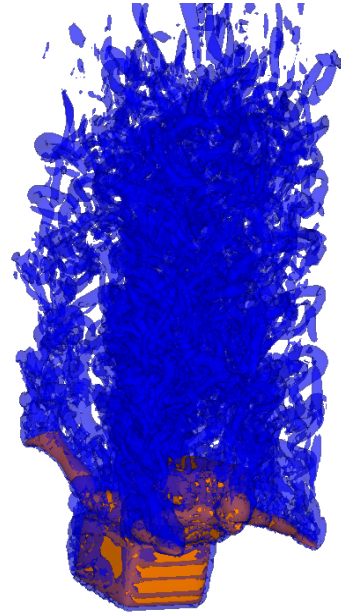
**Figure 3 XY view of the Cartesian volume grid (256 x 128 x 128) with a non-uniform mesh clustered near the MFF configuration. Also shown is the immersed body with its three components: parachutist, chute pack and PDB.**



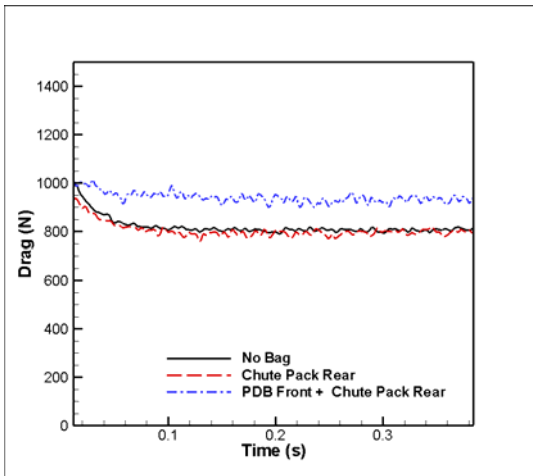
a. Case 1 : Slick Case  
(No Bag)



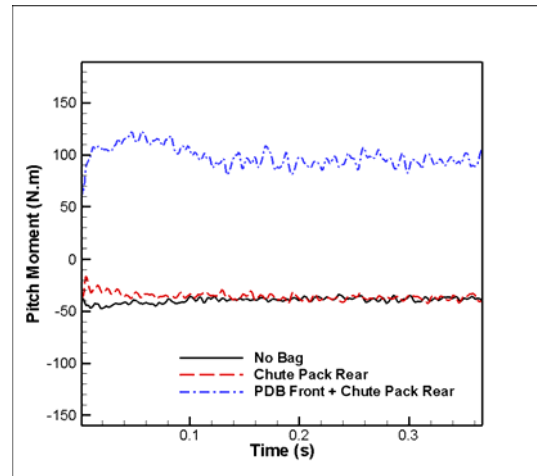
b. Case 2 : Chute Pack Rear



c. Case 3 : PDB Front + Chute Pack Rear



d. Drag Force Comparison



e. Pitching Moment Comparison

**Figure 4 Simulation results for three free fall configurations. Top: Flow structures; Bottom: Drag force and pitching moment on the parachutist.**

### C. Effect of Bag on Aerodynamics

We have performed several MFF simulations at a scaled Reynolds number of  $10^5$ . CartFlow3D requires two distinct meshes: a surface mesh and a volume grid. The surface mesh is composed of triangular elements which are created independently for each object simulated in the flow. Unlike body fitted mesh techniques, intersection regions do not necessitate any special attention. Figure 2 shows surface meshes for three different configurations: Case-1 represents “*slick case*” parachutist body without any bag, Case-2 has a rear back mounted chute pack on the parachutist, and Case-3 corresponds larger front positioned back in addition case 2 model. The same parachutist body surface mesh is used in all simulations; only surface meshes for the bags are set up in the simulations for cases 2 and 3. The same Cartesian volume grid is used in all simulations consisting of  $256 \times 128 \times 128$  cells (or 4.2 Million). An x-y perspective (along  $z=0$  plane) is shown in Figure 3. Mesh clustering near the MFF body with its bag is employed to properly capture the wake dynamics. It should be noted that the current multi-body simulation method is highly suitable for studying the aerodynamic effect of such changes. This also allows using existing surface meshes as well as the same volume grid for all cases which eliminates complicated mesh generation process for each model.

Figure 4 shows the flow structures at zero angle-of-attack (in CFD axes) using the contours of the swirl strength. It is seen that the wake is affected by the presence of the front bag, while the back chute has minimal effect. Figure 4d-e show the comparison of the drag force and pitching moment, respectively for these cases. As it is seen from these figures, the rear chute pack (Case-2) changes the results modestly, as it is in the wake of the body. On the other hand, the large parachutist drop bag (PDB) in front position changes the flow structures and the forces and moments significantly.

## IV. Digital Manikin Module

### A. Functionality and Implementation

The Digital Manikin module has two primary functions:

- Generate the description of the surface geometry of the jumper and equipment in a form appropriate for the CartFlow3D CFD program.
- Generate the mass properties (total mass, cg location, and inertia tensor) for the Dynamics and Control Module.

These two functions are supported by a capability to pose the manikin. Equipment can also be selected and properly positioned with respect to the body.

The Digital Manikin module is built from three software components: HSVS, GEBOD, and Blender. The University of Washington Human Shape Variation Software (HSVVS) generates anthropometrically valid human body shapes in a standard pose for user-specified height, weight, and gender. The Generator of Body Data (GEBOD Version IV<sup>14</sup>) generates joint locations and body segment mass properties for user-specified height and weight. These two programs and their underlying empirical data and statistical models were independently developed from distinct human population samples and focus on different aspects of anthropometry. Blender, a 3D graphics software tool, contains no anthropometric databases but provides a suite of tools for bone structure generation, inverse kinematic (IK) solutions, and 3D object creation and interaction.

The HSVS software generates a description of the human shape in the form of a mesh of polygons. However, there is no skeletal structure, i.e., the joints and bones, which is essential for pose control and estimation of overall mass properties. Thus a method was developed for creating a skeleton automatically given a HSVS-generated human shape. The body segmentation is based on the 17 rigid segments in GEBOD. The first step to replicate the GEBOD segmentation for the HSVS generated human shapes is to locate common anthropometrical landmarks.

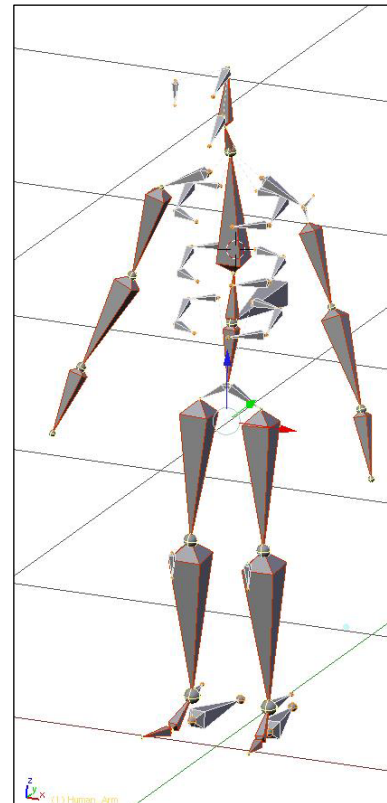
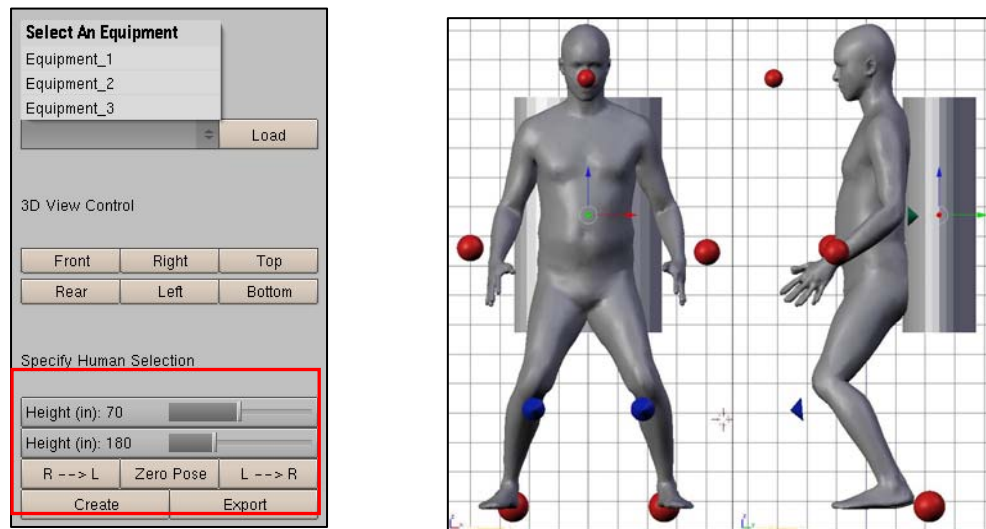


Figure 5 Skeleton template

The skeleton template (Figure 5) was created at STI using the Blender software. The template consists of 17 structure bones (outlined in red) that represent the GEBOD body segments and “skin bones” (outlined in white) that help control the morphing of the body shapes. The bones are positioned and sized by fitting them between the joint locations for the standard HSVS standing pose.

## B. Creating, Posing, Equipping and Saving a Manikin

To create a new manikin, the user firsts selects the desired height and weight using the slider bars in the Digital Manikin graphical user interface GUI and then clicks the “Create” button (Figure 6). The manikin can then be posed graphically by clicking and dragging the hands, feet, or head on the 3-D graphical representation of the manikin. This capability makes use of inverse kinematic features in the Blender software. Once the desired posture has been set, equipment can be attached to define the final configuration. The user selects the desired equipment from the GUI list and clicks “Load” to attach the equipment. The GUI list contains all of the equipment in the equipment database. As shown in Figure 6, a hypothetical barrel-shaped package was loaded and manually placed at the desired position. Since both the human shape and the equipment are treated as rigid, the two objects will overlap instead of deforming when they come in to contact. This simulates the crushing of fabric based equipment. The user can then save the posed, equipped manikin in the manikin database.



**Figure 6 – Digital manikin GUI and Manikin**

## C. Mass Properties

The mass properties computed in the Digital Manikin for the posed, equipped parachutist treated as a rigid body consist of:

- total mass
- location of the center of mass in the manikin
- moments and products of inertia referenced to the center of mass

The mass properties are the primary data to flow from the Digital Manikin to the Dynamics and Control Module. There is an established body of work<sup>13,14</sup> in estimation of mass properties of human body components as functions of basic anthropometric variables. This includes GEBOD which implements a database of human mass property data actually based on a number of earlier studies such as Reference 15. The Digital Manikin module accesses the mass properties of the 17 body segments generated by the GEBOD program. Based on the user’s inputs of height and weight, GEBOD generates anthropometric parameters for each body segment including length, weight, cg location, principle moments of inertia.

The problem of computing the mass properties of the equipped parachutist is well-defined conceptually but complex in the details of relating the parameters from the GEBOD manikin to those of the FAST manikin because the two have slightly different skeletal segment sizes (even for the same nominal height and weight) and a slightly different standard pose. However, reasonable assumptions and approximations were made to allow the GEBOD segment data to be used with the Digital Manikin based on the HSVS shape mesh. The first step is to calculate the mass properties of the Digital Manikin body segments based on the GEBOD data. Then the segment data is summed over all of the segments. Equipment such as rucksacks are treated as additional segments. Further details of the Digital Manikin are presented in Reference 1.

There are three primary coordinate systems used in FAST: Global axes, body axes, and CFD axes. Global axes are used in the definition of the initial manikin shape, the body axes are used for computing the parachutist's dynamics and the CFD axes are used in positioning the manikin in the CarFlow3D CFD grid. The transformations among axis systems are automated in FAST.

## **V. Aerodynamics Module**

### **A. Functionality**

The Aerodynamics Module functions as an interface between the CartFlow3D CFD software and the rest of FAST. Because CartFlow3D, like any CFD code, has much greater computational requirements than the basic FAST code, these two programs run on different computers connected over the Internet. The Aerodynamics Module has two high level functions:

1. Deliver a posed equipped body shape and other necessary parameters to CartFlow3D to initiate a CFD run and
2. Receive data from CartFlow3D after a run and process it for use in flow visualization and in the Dynamics and Control Module.

The Aerodynamics Module also implements a higher level of organization to support the Dynamics and Control Module. For dynamic analysis, CartFlow3D will be used like a wind tunnel. Thus a series of runs for the same manikin configuration with distinct values of angle of attack and sideslip angle for each run will constitute a "test". Each test is made for a fixed body shape, pose and equipment analogous to common practice in aircraft wind tunnel testing. The Aero Module includes basic database features for archiving CFD results. Each database record corresponds to an individual CFD simulation run. The test data sets provide the basis for generating functional relationships (curve fitting) between aerodynamic coefficients and dependent variables such as angle of attack and sideslip angle.

### **B. Positioning the Manikin in the Grid**

CartFlow3D works best if the highest number of grid points are in the  $x$  and  $y$  directions (vertical and horizontal in Figure 3). Consistent with this it is desirable to have the freestream velocity roughly in the direction of the positive CFD  $x$ -axis. This requirement implies that the angles of attack and sideslip with respect to the CFD  $x$ -axis should be rather small. Further the CFD  $y$ -axis should be roughly aligned with the longest dimension of the body and normal to the  $x$ -axis. Thus for the initial FAST applications, which are focused on the MFF equilibrium descent, the body should be roughly oriented to the CFD axes as shown in Figure 3.

A key advantage of FAST, made possible by the IBM formulation of CartFlow3D, is that the same CFD grid can generally be used for multiple manikin runs and even multiple tests. This is possible because of the assumption that the orientation of the freestream velocity with respect to the manikin will always be close to the equilibrium freefall condition. While provision to adjust the grid is available, using a single grid provides a major simplification for many FAST applications.

Even with a fixed grid, it is necessary to insure that the manikin is appropriately placed inside the fine region of the grid. This requires defining gross dimensions of the manikin which is done by placing an imaginary rectangular "bounding box" around the manikin. The bounding box is sized to just contain the posed, equipped manikin. The centroid of the bounding box is centered horizontally in the CFD grid typically about a quarter of the way above the bottom. The Aerodynamics Module also calculates the manikin cg location in the CFD axes. CartFlow3D then calculates the moments about the cg. In the above process the mesh points defining the manikin body and equipment shapes are automatically transformed from the body axes used in dynamics analysis to the CFD axes.

### C. Initiating CFD Runs and Accessing the CFD Data

The Aero Module steps noted above are automatically performed in FAST. The FAST user does have to input some variables to initiate runs. The most basic of these are angle of attack, angle of sideslip and airspeed. The boundary condition velocity components (in CFD axes) are automatically computed from the angles of attack  $\alpha$  and sideslip  $\beta$  (with respect to the body axes) and airspeed input by the user through the GUI.

Considerable data is generated in each CartFlow3D run. Much of this is flow field data analyzed with the commercial Tecplot software which has been integrated with FAST. With respect to the Dynamics and Control Module, the primary data required are the six aerodynamic force and moment coefficients. These are generated in CartFlow3D from the force and moment components in the CFD axes. The transformations of the aerodynamic force and moment coefficients from CFD axes to body axes are performed automatically in the Aero Module. When a series of CFD runs have been made according to a test plan, each force and moment coefficient data set can be fitted to generate approximate analytic functions of the independent variables (angles of attack and sideslip in body axes). Use of analytic functions simplifies generation of partial derivatives for calculating stability derivatives. Data points and fitted curves (second order polynomials) are shown in Figure 7 for initial runs for a manikin with chute pack alone similar to that shown Figure 2.

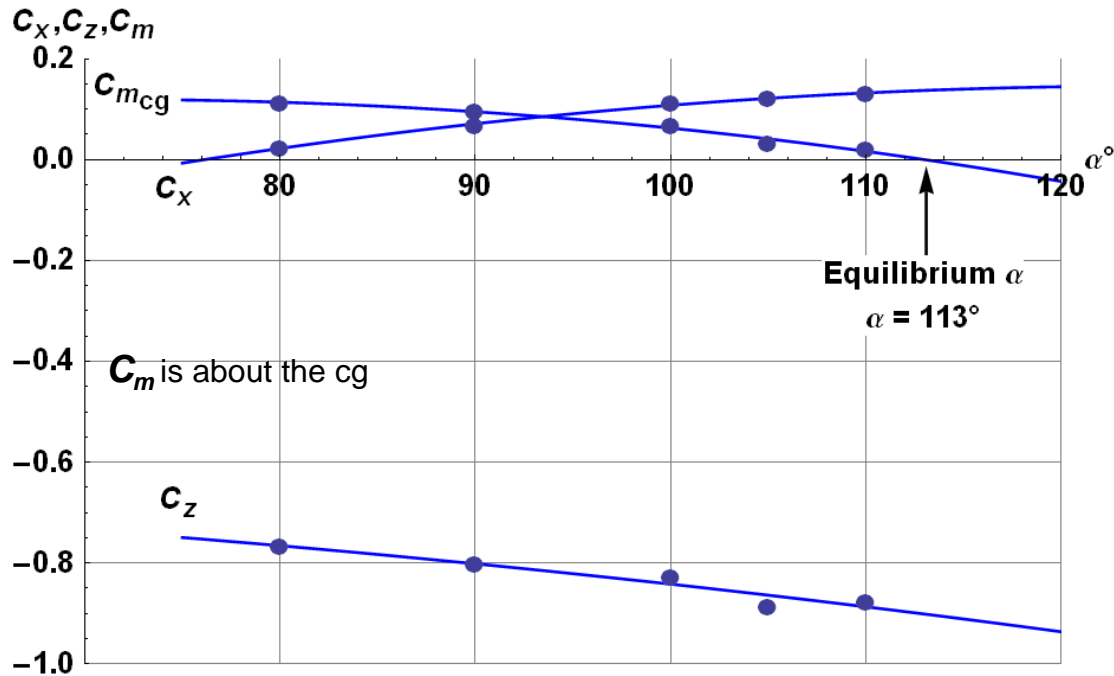


Figure 7 Aerodynamic coefficient data and fitted curves

## VI. Dynamics and Control Module

### A. Overview

The Dynamics and Control module provides the means for predicting how the aerodynamics, obtained from CFD, will affect the motion of the free fall parachutist. Aircraft stability and control analysis<sup>16</sup> provides a precedent for addressing this problem, although there are important distinctions between the dynamics of freefall parachutists and airplanes. The military free fall manual<sup>17</sup> implies that the parachutist exits the airplane in a more-or-less vertical attitude and then maneuvers to a horizontal position for steady descent (Figure 8) from which the parachute is opened. These initial free fall maneuvers may be complex and the parachutist may not behave as a rigid body. Even if a rigid body approximation is reasonable, nonlinear simulation of large amplitude maneuvers will not generally be

practical because of the extreme amount of computational time required to generate CFD data over a wide range of angle of attack and sideslip. Thus the FAST Dynamics and Control Module has been initially focused on small perturbation linearized dynamic analysis about the equilibrium freefall condition with the manikin assumed rigid.

### B. Equilibrium Conditions

The fundamental criterion for equilibrium is that the pitching moment coefficient  $C_m(\alpha)$  at the center of gravity is zero. From the  $C_m(\alpha)$  curve of Figure 7 the trim angle of attack is about  $\alpha_0 = 115^\circ$ . The flight path angle (angle from the horizon to the velocity vector) in equilibrium  $\gamma_0$  is given by

$$\gamma_0 = -\frac{\pi}{2} + \tan^{-1}\left(\frac{C_L}{C_D}\right) = -104^\circ$$

where the lift and drag coefficient functions are shown in Figure 9. Note that the  $C_L$  is negative around the trim angle of attack. The pitch attitude (angle between the body  $x$ -axis and the horizon) is  $\Theta_0 = \alpha_0 + \gamma_0 = 8.7^\circ$ .

This solution and its implications are most easily seen in Figure 10. First the parachutist is gliding slightly backwards. This is not to say that an actual parachutist would establish this equilibrium condition. It's probably more correct to say that a rigid dummy of this shape and weighted to this CG would achieve this equilibrium and would fly backwards. It may be that a slight change in pose will change the relationship between the angle of attack for  $C_L = 0$  and the trim  $\alpha_0$  so that the descent will be vertical or even slightly forward. However, the pitch attitude indicates that the parachutist is nearly horizontal as he should be in equilibrium descent.

### C. Formulation of Linearized Longitudinal Dynamics

For a free fall parachutist treated as a rigid body with small perturbations in body motion, the linearized equations of motion are basically similar to the standard formulations used in aircraft dynamics<sup>16</sup>. However, linear analysis is usually applied to aircraft in low angle of attack trim conditions where the momentum wake is relatively small. For application to free fall, linear analysis will be applied to the steady descent case with high angle of attack and a very wide wake comparable to an aircraft in a flat spin. The primary distinction between aircraft and the free fall parachutist will be seen in the characteristics of the aerodynamic stability derivatives ( $Z_w, M_q$ , etc.). There is of course a vast knowledge base for aircraft stability derivatives, but there is nothing comparable for the free fall parachutist. The latter situation can be greatly improved through extensive use of FAST/CartFlow3D.

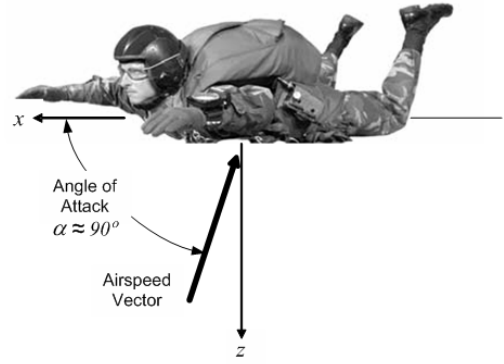


**Figure 8. Parachutist in Nominal Free Fall Configuration [17]**

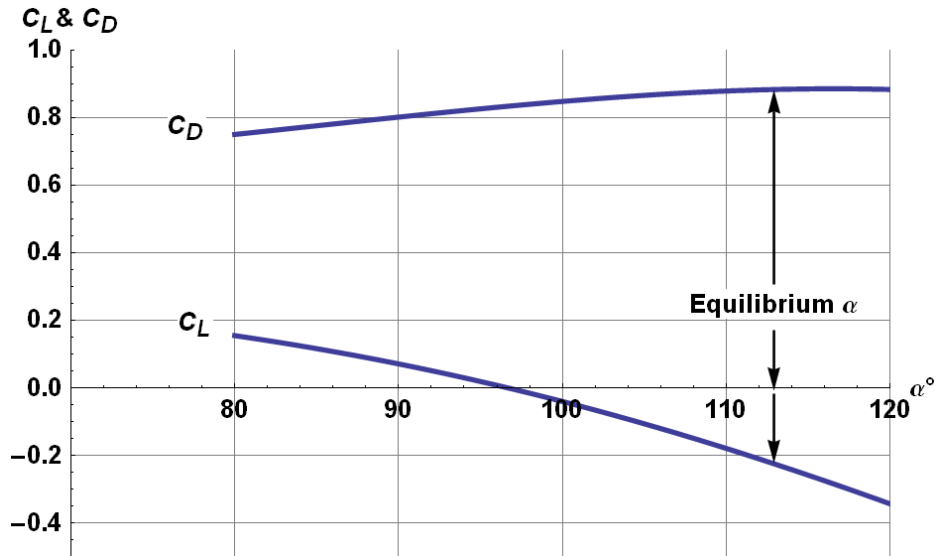


Figure 9 Lift and drag coefficient curves

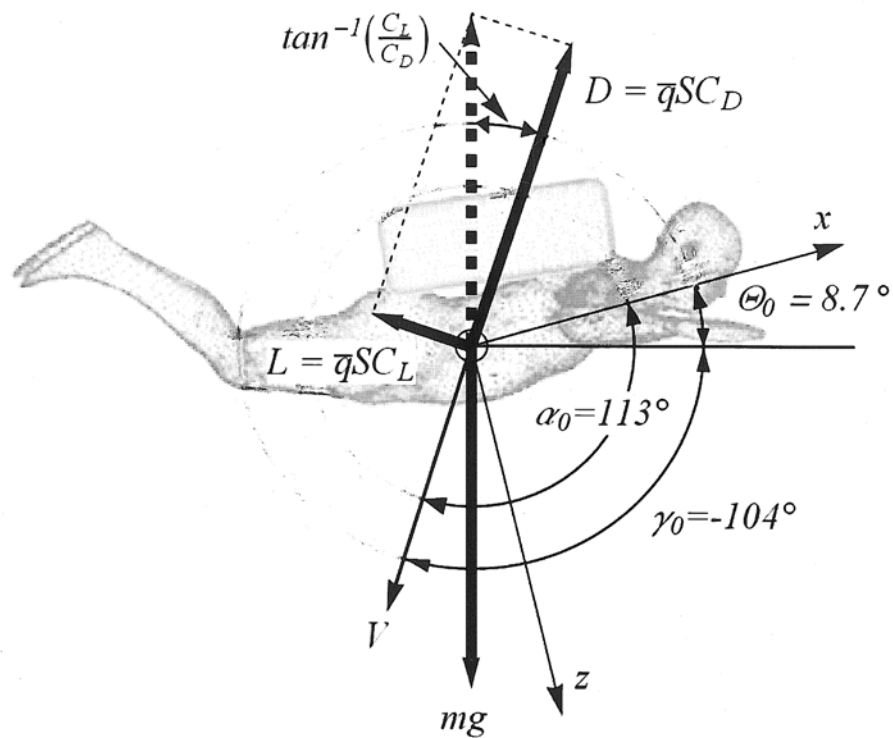


Figure 10 Equilibrium descent condition

The standard formulation of the dimensional stability derivatives<sup>16</sup> must be adapted to the high angle of attack condition typical of MFF. Here the equations of motion will be developed in body axes rather than stability axes. By way of example, the development is illustrated for the heave derivative  $X_w$

$$\begin{aligned} X_w &= \left. \frac{1}{m} \frac{\partial X}{\partial W} \right|_{V=V_0} = \left. \frac{\rho S}{2m} \frac{\partial}{\partial W} \left( (U^2 + W^2) C_x \right) \right|_{V=V_0} \\ &= \left. \frac{\rho S V_0}{m} \left( \frac{W_0}{V_0} C_x + \frac{V_0}{2} \frac{\partial C_x}{\partial W} \right) \right|_{V=V_0} \end{aligned}$$

The derivative  $\left. \frac{\partial C_x}{\partial W} \right|_{V=V_0}$  must now be related to angle of attack as

$$\begin{aligned} \frac{\partial C_x}{\partial W} &= \left. \frac{\partial C_x}{\partial \alpha} \frac{\partial \alpha}{\partial W} \right|_{V=V_0} = \left. \frac{\partial C_x}{\partial \alpha} \frac{\partial}{\partial W} \tan^{-1} \left( \frac{W}{U} \right) \right|_{V=V_0} \\ &= \left. \frac{\partial C_x}{\partial \alpha} \frac{1}{1 + (W/U)^2} \frac{\partial}{\partial W} \left( \frac{W}{U} \right) \right|_{V=V_0} = \left. \frac{U_0}{V_0^2} \frac{\partial C_x}{\partial \alpha} \right|_{V=V_0} \end{aligned}$$

Thus

$$X_w = \left. \frac{\rho S V_0}{m} \left( \frac{W_0}{V_0} C_x + \frac{U_0}{2V_0} C_{x_\alpha} \right) \right|_{V=V_0}$$

#### D. Pitch Rate and Heave Acceleration Derivatives

The pitch rate derivatives  $X_q, Z_q, M_q$  are difficult to measure in a wind tunnel, because the model must be rotated and it is generally difficult to separate the  $q$  and the  $\dot{\alpha}$  effects. Physically this is best done in a whirling arm apparatus in which the model is rotated, at constant angle of attack, about a point away from the model. In any case it is currently not feasible to compute pitch rate derivatives using CartFlow3D because the model cannot rotate through the CFD grid. Thus  $X_q, Z_q, M_q$  are treated as variables to adjust the modal damping based on estimates of the corresponding nondimensional derivatives. Only  $M_q$  is expected to be significant.

The heave acceleration derivatives  $X_{\dot{w}}, Z_{\dot{w}}, M_{\dot{w}}$  arise from unsteady aerodynamic effects. For aircraft,  $X_{\dot{w}}$  and  $Z_{\dot{w}}$  are generally considered negligible but significant  $M_{\dot{w}}$  can result from lift induced on the tail. This would not apply to freefall, however, unsteady aerodynamic effects can be important in bluff bodies, the most notable example being apparent mass effects on submarines and airships. But the significance of these effects depends on the low density of such buoyant vehicles. The high density of the parachutist compared to atmospheric density would render apparent mass terms insignificant. Thus all of these derivatives are neglected for free fall.

#### E. Linearized Longitudinal Dynamics

Dynamics and Control Module calculations are as follows:

- Compute  $U_0, W_0$

$$U_0 = V_0 \cos \alpha_0, \quad W_0 = V_0 \sin \alpha_0$$

- Compute stability derivatives

$$\begin{aligned}
X_u &= \frac{\rho S V_0}{m} \left( \frac{U_0}{V_0} C_{X'}(\alpha_0) - \frac{W_0}{2V_0} C_{X_{\alpha'}}(\alpha_0) \right) & X_w &= \frac{\rho S V_0}{m} \left( \frac{W_0}{V_0} C_{X'}(\alpha_0) + \frac{U_0}{2V_0} C_{X_{\alpha'}}(\alpha_0) \right) \\
Z_u &= \frac{\rho S V_0}{m} \left( \frac{U_0}{V_0} C_{Z'}(\alpha_0) - \frac{W_0}{2V_0} C_{Z_{\alpha'}}(\alpha_0) \right) & Z_w &= \frac{\rho S V_0}{m} \left( \frac{W_0}{V_0} C_{Z'}(\alpha_0) + \frac{U_0}{2V_0} C_{Z_{\alpha'}}(\alpha_0) \right) \\
M_u &= \frac{\rho S V_0 c}{I_y} \left( \frac{U_0}{V_0} C_M(\alpha_0) - \frac{W_0}{2V_0} C_{M_{\alpha}}(\alpha_0) \right) & M_w &= \frac{\rho S V_0 c}{I_y} \left( \frac{W_0}{V_0} C_M(\alpha_0) + \frac{U_0}{2V_0} C_{M_{\alpha}}(\alpha_0) \right)
\end{aligned}$$

$$X_q \approx 0, Z_q \approx 0, M_q = \text{adjustable}, \quad X_{\dot{w}} \approx Z_{\dot{w}} \approx M_{\dot{w}} \approx 0$$

- Compute the dynamics matrix,  $A$

$$A = \begin{bmatrix} X_u & X_w & (X_q - W_0) & -g \cos \Theta_0 \\ Z_u & Z_w & (U_0 + Z_q) & -g \sin \Theta_0 \\ M_u & M_w & M_q & 0 \\ 0 & 0 & 1 & 0 \end{bmatrix}$$

Evaluating the dynamics matrix using the curves of Figure 7,  $M_q = 0$ , and the mass properties of the manikin.

$$A = \begin{bmatrix} -0.0286 & 0.0341 & -158.6 & -31.8 \\ 0.1488 & -0.240 & -67.4 & -4.85 \\ 0.1576 & 0.0670 & 0 & 0 \\ 0 & 0 & 1 & 0 \end{bmatrix}$$

Solving the system  $(sI - A)x = 0$  yields two complex eigenvalues, one stable and one unstable:

$$(0.0929 \pm 5.43j, -0.227 \pm 0.0330j)$$

The stable (left half of the s-plane) root is lower frequency (0.227 rad/sec) and well damped (very close to the real axis.) The much higher frequency (5.43 rad/sec) mode is very near the imaginary axis and unstable for the nominal  $M_q = 0$ . However, this root moves to the imaginary axis (neutral stability) if the pitch damping is increased by setting  $M_q = -0.2 \text{ sec}^{-1}$ . Clearly this complex mode is essentially the body pitch dynamics and is roughly analogous to the aircraft short period mode.

The heavily damped, low frequency, complex mode is the coalescence of the heave and surge subsidence modes. These can be understood by considering the dynamics of a sphere falling in equilibrium. By symmetry it will have no pitch dynamics. If an impulse is applied vertically upward, the sphere's descent will be slowed to below the equilibrium velocity. This will decrease the drag so that the excess of gravity will reaccelerate the sphere to equilibrium as a first order lag. The inverse time constant for this dynamic can be shown to be  $\rho V_0 S C_D / m$ . For the

parameters of the above parachutist this yields 0.273 rad/sec, which is quite close to the frequency of the low frequency mode above. It is tempting to compare the freefall mode to the phugoid mode of an airplane. The “3DOF” approximation of the phugoid natural frequency<sup>16</sup>, when evaluated for the freefall parameters, is  $\sqrt{2g/V_0} = 0.264$  rad/sec which again is close to the freefall heave-surge subsidence modal frequency. However, airplanes in normal flight tend to have much lower phugoid damping ratios which indicates that “humans don’t fly just like airplanes.”

### Acknowledgments

This work was supported by the U. S. Army, Natick Soldier Research, Development and Engineering Center, Natick, MA.

### References

- 
- <sup>1</sup> Myers, T.T., R. Mittal, et al, “Free Fall Analysis and Simulation Tool (FAST)”, *20th AIAA Aerodynamic Decelerator Systems Technology Conference and Seminar*, 4-7 May 2009, Seattle
  - <sup>2</sup> Mittal, R., and Iaccarino, G., “Immersed Boundary Methods,” *Annual Review of Fluid Mechanics*, Vol. 37, 2005, pp. 239-261
  - <sup>3</sup> Vreman, A., “An Eddy Viscosity Subgrid-scale Model for Turbulent Shear Flow: Algebraic Theory and Applications,” *Physics of Fluids*, Vol. 16, 2004, pp. 3670–3680
  - <sup>4</sup> You, D. and Moin, P., “A Dynamic Global-Coefficient Subgrid-Scale Eddy-Viscosity Model for Large-Eddy Simulation In Complex Geometries,” *Physics of Fluids*, Vol. 19, 065110 (2007).
  - <sup>5</sup> Craley, J. and K. J. Desabrais, “An Investigation of Pilot Parachute Deployment Hesitation”, AIAA 2007-2575, 2007.
  - <sup>6</sup> Osher, S., Fedkiw R. P., "Level set methods – an overview and some recent results", *J. Comput. Phys.*, Vol. 169, 2001, pp. 463–502, 2001
  - <sup>7</sup> Tran, L. B. and Udaykumar, H. S., “A Particle-level set-based Sharp Interface Cartesian Grid Method for Impact, Penetration, and Void Collapse,” *J. Comput. Phys.*, Vol. 193, 2004, pp. 469–510
  - <sup>8</sup> Smagorinsky, J., “General Circulation Experiments with Primitive Equations,” *Mon. Weather Rev.*, Vol. 91, 1963
  - <sup>9</sup> Driest, E. V., “On Turbulent Flow near a Wall”, *Journal of Aerospace Science*, Vol. 23, 1956.
  - <sup>10</sup> Germano, M., “A Dynamic Subgrid Scale Eddy-Viscosity Model,” *Physics of Fluids*, Vol. 3, 1991, pp. 1760
  - <sup>11</sup> Meneveau, C., Lund, T., and Cabot, W., “A Lagrangian Dynamic Subgrid Scale Model of Turbulence,” *Journal of Fluid Mechanics*, Vol. 319, 1996, pp. 353–385.
  - <sup>12</sup> Ramakrishnan, S., Zheng, L., Mittal, R. and Najjar, F., “Large-Eddy Simulation of Flows with Complex Moving Boundaries: Application to Flying and Swimming in Animals,” *38th AIAA Fluid Dynamics Conference and Exhibit*, 2009, AIAA-2009-3976.
  - <sup>13</sup> Webb Associates, “Anthropometric Source Book, Vol. I: Anthropometry for Designers”, NASA RP 1024, 1978
  - <sup>14</sup> Cheng, H., et al, “Generator of Body (GEBOD) Manual”, AL/CF-TR-1994-0051, March 1994
  - <sup>15</sup> McConville, J. T. and T. D. Churchill, “Anthropometric Relationships of Body and Body Segment Moments of Inertia”, AFARMRL-TR-80-119, December 1980.
  - <sup>16</sup> McRuer, D. T., Ashkenas, I. L., and Graham, D., *Aircraft Dynamics and Automatic Control*, Princeton University Press, 1973
  - <sup>17</sup> Anon., “Special Forces Military Free-Fall Operations”, U.S. Army, FM 3-05.211, April 2005